

Direct Search signal of two-component Dark Matter

Subhaditya Bhattacharya,^a Dipankar Pradhan.^a

^a*Department of Physics, Indian Institute of Technology Guwahati,
North Guwahati, Assam-781039, India.*

E-mail: subhab@iitg.ac.in, d.pradhan@iitg.ac.in

ABSTRACT: How do we know if the dark sector consists of more than one dark matter (DM) component is an important question, for which the answer is not very definite. In this article we study such a possibility in context of direct DM search. It was pointed out earlier in a model independent analysis that a kink in the nuclear recoil energy spectrum may indicate to the presence of two DM components. However, realising one such model was difficult due to experimental constraints. Here we propose and study a model containing a vector boson DM and a scalar DM, aided by a light scalar mediator, where a kink in the nuclear recoil spectrum arises after addressing individual relic densities, direct search limits, collider constraints and theoretical limits. We find out the allowed parameter space of the model and those regions likely to show such distinctive signal.

KEYWORDS: Models for Dark Matter, Particle Nature of Dark Matter, Specific BSM Phenomenology.

Contents

1	Introduction	1
2	The Model	3
3	Coupled Boltzmann Equation and Relic density	7
4	Two component dark matter signal in direct detection	9
5	Summary and conclusions	12
A	Feynman diagrams for DM relic density	14
B	Thermal equilibrium for h_2	15

1 Introduction

Albeit the hints from astrophysical and cosmological observations that our observed universe contains 26.8% [1, 2] dark matter (DM), its detection is yet to be achieved. Apart from the stability, massive nature and electromagnetic charge neutrality, we remain largely nescience about DM characteristics. One particular question is often asked whether the dark sector consists of a single particle or many, like the visible sector does. And if so, then how the observations related to relic density, and search strategies alter. This is one of the points of study in this paper.

When the DM freezes out of thermal bath, gives rise to WIMP [3–6] or SIMP [7] type candidates, while FIMP [8] is produced non-thermally. Apart, several possibilities exist. In multicomponent frameworks, DM-DM interaction is constrained from galaxy cluster observations [9–13]. WIMP-WIMP [14, 15] scenario has best detectability as WIMP has sizeable DM-SM interaction, while WIMP-FIMP [16], FIMP-FIMP [17, 18], SIMP-SIMP [19, 20], WIMP-pFIMP¹ [21–24], SIMP-pFIMP [25] frameworks offer plenty of phenomenology.

DM search mainly relies on the DM-SM interaction and is done mainly via three strategies, direct, indirect and collider searches. With minimal electromagnetic coupling, DM misses the detector, and produces missing momenta or energy. We cite some example signal/background analysis at upcoming colliders, like HL-LHC [26], FCC [27], CEPC [28], muon collider [29], ILC [30] etc. Occasionally, the collider may also probe the mediator for the interaction between DM and SM, see [31]. Non observation of DM at collider put bounds on DM-SM interaction and mass, the ones relevant include Tevatron [32], LEP [33]

¹Pseudo-FIMP (pFIMP) arises in a multi-component DM frameworks, having feeble connection to SM, but adequate interaction with the partner DM.

and LHC [34]. Indirect detection (ID) relies on excess of SM particles (e.g., charged leptons, gamma rays, neutrinos, protons, anti-particles etc.) produced by the decay or annihilation of DM particles [35] in regions with high DM density, such as the Galactic Center and dwarf spheroidal galaxies. Indirect searches provide constraints on DM self-annihilation and semi-annihilation, for eg., Fermi-LAT [36, 37], H.E.S.S [38], and CTA [39]. In direct detection (DD), DM scatters off the detector nuclei or atomic electrons (depending on mass), and results in recoil of the nuclei/electrons producing scintillation signal in the detector [40, 41]. As our focus here is on cold DM in the GeV-TeV mass range, which plays a crucial role in supporting the universe’s structure formation, DM produces nuclear recoil. The most relevant constraints in such cases are derived from experiments such as PandaX-xT [42], XENONnT [43], LUX-ZEPLIN [44], and XLZD [45] amongst others. Heavy DM search is also underway with XENONnT [46] and sub-GeV DM searches with SuperCDMS [47–49], EDELWEISS [50], CRESST-III [51], DarkSide-50 [52], CDEX-10 [53], DAMIC-M [54], SENSEI [55], etc.

In a model-independent analysis of two-component DM setup [56, 57],² it was shown that a kink may appear in the recoil energy spectrum of DD, when one DM is of low mass ~ 10 GeV, and the other is heavy, $\gtrsim 40$ GeV. The only physical observable in the event rate analysis is the curvature of the event rate spectrum, which would serve as evidence for the presence of more than one DM particle in the dark sector. The position and properties of this curvature depend not only on the DM masses but also on local DM densities and the DM scattering rates with detector nuclei. The study motivated us to look into a UV complete set up where such observations can be realised. This is challenging as having a low mass WIMP faces severe constraint from experimental data, particularly invisible decay constraints of Higgs or the DM-SM portal. Further, the relative relic densities and DM masses are closely related in a realistic model, so that finding a parameter space where such novel feature can be seen in future sensitivities of DD becomes an interesting exercise.

In this work, SM is extended by a gauge singlet vector boson DM (VBDM), which acquires mass through the spontaneous breaking of a $U(1)_X$ symmetry via a complex scalar. Apart we postulate the presence of a real scalar DM (RSDM). The stability of both is ensured by an appropriate $\mathcal{Z}_2 \otimes \mathcal{Z}'_2$ symmetry. Through the mixing with CP-even part of the SM Higgs doublet, a new real scalar particle emerges along with the SM Higgs [61, 62], playing a crucial role in the analysis. Our goal is to study the allowed parameter space satisfying relic density, DD, ID, and the collider constraints, that result in a visible kink in the total event rate spectrum indicating the presence of more than one DM components.

This paper is organized as follows: in Section . 2, we discussed the possibility of getting two stable vector and scalar DM components transforming under a single $\mathcal{Z}_2 \otimes \mathcal{Z}'_2$ symmetry and in Section . 3 we have discussed the coupled Boltzmann equation and its solution- relic density of DMs. The direct detection signal for this vector-scalar DM model is discussed in Section . 4. We finally summarise in Section . 5. Appendix A, and B provide some necessary details omitted in the main text.

²In context of colliders, references [58, 59] have shown that a two-component DM scenario can lead to the appearance of two peaks in the missing energy (\cancel{E}) distribution; reference [60] attempted to explore how the indirect signal (specifically the photon flux) is altered in the presence of two DMs.

2 The Model

This article aims to come up with a UV-complete model that produces a visible kink in the time-averaged event rate spectrum while satisfying all the current theoretical and observational constraints. Its worth mentioning that all the simple minded two component DM models, consisting of singlet or doublet scalar or fermion, leaves in a mass regime where such distinguishability is difficult to address.

To alleviate this, we extend the SM gauge symmetry by a global $U(1)_X$ symmetry under which the complex scalar S is charged. The associated dark gauge boson X_μ is stabilized by a \mathcal{Z}_2 symmetry, making it a viable vector boson DM candidate. We further include a real scalar ϕ singlet, stable under a \mathcal{Z}'_2 symmetry, representing a second DM candidate. The charges of these particles under the $\mathcal{Z}_2 \otimes \mathcal{Z}'_2$ symmetry are listed in tab. 1. The SM

Dark Fields	$\mathcal{Z}_2 \otimes \mathcal{Z}'_2$	
Real scalar ϕ	ϕ	$-\phi$
Complex scalar S	S^*	S
$U(1)_X$ Gauge Boson X_μ	$-X_\mu$	X_μ

Table 1: Model particles and their charges under $\mathcal{Z}_2 \otimes \mathcal{Z}'_2$ symmetry.

extended dark sector Lagrangian is written as [63],

$$\mathcal{L} = \mathcal{L}_{\text{SM}} + |\partial_\mu \phi|^2 + |D_\mu S|^2 + \frac{1}{4} X_{\mu\nu} X^{\mu\nu} - V(\phi, S, H), \quad (2.1)$$

where,

$$D_\mu = \partial_\mu + ig_X X_\mu; \quad X_{\mu\nu} = \partial_\mu X_\nu - \partial_\nu X_\mu;$$

and,

$$\begin{aligned} V(\phi, S, H) = & -\mu_H^2 (H^\dagger H) + \lambda_H (H^\dagger H)^2 + \frac{1}{2} \mu_\phi^2 \phi^2 + \frac{1}{4!} \lambda_\phi \phi^4 - \mu_S^2 (S^* S) + \lambda_S (S^* S)^2 \\ & + \frac{1}{2} \lambda_{\phi H} \phi^2 (H^\dagger H) + \frac{1}{2} \lambda_{\phi S} \phi^2 (S^* S) + \lambda_{HS} (H^\dagger H) (S^* S). \end{aligned} \quad (2.2)$$

The potential $V(\phi, S, H)$ in eq. 2.2, for $\lambda_H, \lambda_S, \lambda_\phi, \mu_\phi^2 > 0$ and $\mu_H^2 < 0, \mu_S^2 < 0$, so that it provides the following vacuum:

$$H = \begin{pmatrix} \phi^+ \\ \frac{v+h+i\phi_0}{\sqrt{2}} \end{pmatrix} \rightarrow \langle H \rangle = \begin{pmatrix} 0 \\ \frac{v}{\sqrt{2}} \end{pmatrix}; \quad (2.3)$$

$$S = \frac{v_s + s + i\mathcal{A}}{\sqrt{2}} \rightarrow \langle S \rangle = \frac{v_s}{\sqrt{2}}; \quad \langle \phi \rangle = 0. \quad (2.4)$$

In the above, $\phi^{\pm,0}$, \mathcal{A} denote Nambu-Goldstone Bosons [64–67], which disappear in the unitary gauge after EWSB. The breaking of $U(1)_X$ makes the associated gauge boson massive:

$$m_X = v_s g_X, \quad (2.5)$$

where g_X denotes $U(1)_X$ gauge coupling constant and v_s denotes the $U(1)_X$ symmetry breaking scale. Let us have a quick look into the relevant constraints.

• Tree level unitarity

The tree-level unitarity of the theory comes from all possible $2 \rightarrow 2$ scattering amplitude and can be ensured by [68, 69],

$$\lambda_H < 4\pi, \quad \lambda_S < 4\pi, \quad \lambda_{HS} < 8\pi. \quad (2.6)$$

• Perturbativity

To maintain the perturbativity of the theory, the couplings of the theory obey [70],

$$\lambda_H < 4\pi, \quad \lambda_S < 4\pi, \quad g_X < \sqrt{4\pi}, \quad \lambda_{HS} < 4\pi. \quad (2.7)$$

• Limits on the thermal Dark Matter mass

There is a unitarity bound that sets an upper limit on the mass of symmetric and asymmetric thermal DM, is ~ 110 TeV [71–74]. The combined Big Bang Nucleosynthesis (BBN) and Cosmic Microwave Background (CMB) provides the lower limits to the WIMP masses is $\sim 0.5 - 5$ MeV [75–83].

• Relic density

The Planck data [1] constrains the present DM relic density,

$$\Omega_{\text{DM}} h^2 = 0.1200 \pm 0.0012. \quad (2.8)$$

where h is the reduced Hubble parameter $H_0/(100 \text{ km/s/Mpc})$ with $H_0 = 67.4 \pm 0.5 \text{ km/s/Mpc}$ being the current Hubble constant.

• Ranges of mixing angle ϑ

As the scalar mass matrix is real, symmetric and non-diagonal, it can be diagonalised by an orthogonal matrix, resulting in mass eigenstates (h_1, h_2) .

$$\begin{pmatrix} h_1 \\ h_2 \end{pmatrix} = \begin{pmatrix} \cos \vartheta & -\sin \vartheta \\ \sin \vartheta & \cos \vartheta \end{pmatrix} \begin{pmatrix} h \\ s \end{pmatrix}. \quad (2.9)$$

Here we assume h_1 to be SM like, and h_2 is lighter. The relations between the parameters in the Lagrangian, to the physical ones and mixing are,

$$\mu_H^2 = (\lambda_H v^2 + \frac{1}{2} \lambda_{HS} v_s^2), \quad (2.10)$$

$$\mu_S^2 = (\lambda_S v_s^2 + \frac{1}{2} \lambda_{HS} v^2), \quad (2.11)$$

$$\lambda_{HS} = \frac{\sin 2\vartheta}{2v_s v} (m_{h_2}^2 - m_{h_1}^2), \quad (2.12)$$

$$\lambda_H = \frac{1}{2v^2} (m_{h_1}^2 \cos^2 \vartheta + m_{h_2}^2 \sin^2 \vartheta), \quad (2.13)$$

$$\lambda_S = \frac{1}{2v_s^2} (m_{h_2}^2 \cos^2 \vartheta + m_{h_1}^2 \sin^2 \vartheta). \quad (2.14)$$

The Higgs precision measurement set an upper limit on the $h-s$ mixing angle ϑ at 95% CL for 125.1 GeV Higgs [84–91],

$$|\sin \vartheta| \lesssim 0.29. \quad (2.15)$$

In our analysis, we have chosen a small but not overly tiny mixing angle ($10^{-4} \lesssim |\sin \vartheta| \lesssim 10^{-2}$), ensuring h_2 stays in thermal equilibrium during DM freeze-out, has a lifetime shorter than the BBN era ($\tau_{h_2} < 1$ sec), and does not disrupt BBN or induce invisible Higgs decays.

• Higgs invisible decay

If DM's connected via Higgs portal, have smaller mass than half of the SM Higgs, then Higgs can invisibly decay to DM pair. The most sensitive limits on $\mathcal{B}_{h_1 \rightarrow \text{inv}}$ are obtained in VBF searches exploring data collected at $\sqrt{s} = 13$ TeV, excluding $\mathcal{B}_{h_1 \rightarrow \text{inv}} < 0.18$ (0.10) observed (expected) at 95% C.L using 138 fb $^{-1}$ of CMS data, [92], and $\mathcal{B}_{h_1 \rightarrow \text{inv}} < 0.15$ (0.10) using 139 fb $^{-1}$ of ATLAS data [93]. Together, searches for invisible decays of the Higgs boson using 139 fb $^{-1}$ of $p p$ collision data at $\sqrt{s} = 13$ TeV recorded in Run 2 data of LHC set an upper limit on the invisible Higgs boson branching ratio of $\mathcal{B}_{h_1 \rightarrow \text{inv}} < 0.113$ ($0.080_{-0.022}^{+0.031}$) observed (expected) at the 95% CL. Here we assume that the dark Higgs h_2 decays instantaneously inside the detector, with DMs long-lived. In our context, therefore, the invisible decay width of the SM Higgs is,

$$\Gamma_{h_1}^{\text{inv}} = \frac{\mathcal{B}_{h_1 \rightarrow \text{inv}}}{1 - \mathcal{B}_{h_1 \rightarrow \text{inv}}} \Gamma_{h_1}^{\text{SM}}, \quad (2.16)$$

where, $\Gamma_{h_1}^{\text{inv}} = \Gamma_{h_1 \rightarrow \text{XX}} + \Gamma_{h_1 \rightarrow h_2 h_2}$ and $\Gamma_{h_1}^{\text{SM}} = 4.100 \times 10^{-3}$ GeV ($\pm 1.4\%$) [94] for $m_{h_1} = 125.09$ GeV.

• Can h_2 be a 95 GeV scalar?

The latest CMS analysis confirms an excess of di-photon events around 95 GeV. By combining data from the first three years of Run 2, collected at $\sqrt{s} = 13$ TeV with integrated

luminosities of 36.3 fb^{-1} , 41.5 fb^{-1} , and 54.4 fb^{-1} , CMS reports a local (global) significance of 2.9 (1.3) σ at a mass of 95.4 GeV [95]. In contrast, ATLAS reported di-photon search results below 125 GeV using 80 fb^{-1} of Run 2 data [96] to show only a mild excess, with the largest deviation at 95.4 GeV , yielding a local significance of 1.7σ [97]. A combined analysis gives a signal strength of $\mu_{\gamma\gamma}^{\text{ATLAS+CMS}} = 0.24_{-0.08}^{+0.09}$ [98], corresponding to a 3.1σ excess. Some studies explored the possibility with $U(1)_X$ gauge boson DM model, containing a real scalar h_2 along with the SM Higgs h_1 [99], investigating the processes $q\bar{q} \rightarrow t\bar{t}X_\mu X^\mu$ and $q\bar{q} \rightarrow VX_\mu X^\mu$ with $V \rightarrow \ell\bar{\ell}$, with $m_{h_2} = 95.4 \text{ GeV}$ and $V = Z_\mu, h_1$. No exclusions apply to our region of interest, provided that $g_X < 10^{-2}$ and $|\sin\vartheta| < 10^{-2}$. The reference [100] provides theoretical predictions for signal strengths in $\gamma\gamma$, $\tau\bar{\tau}$, and $b\bar{b}$ channels in the $U(1)_X$ SSM model, which aligns well with the excesses observed by CMS. Interestingly, LEP data strongly disfavours the production of 95 GeV scalar particle, as well as any other new physics interpretation in the $95\text{--}100 \text{ GeV}$ mass range [101]. We do not intend to perform a full analysis of h_2 to diphoton decay, which can cause this excess near 95 GeV .

• Bounds on light mediator h_2 mass from thermalization condition

The decay or annihilations of the light scalar h_2 into SM fermions is restricted by BBN data, because the precision measurement of the baryon density through BBN and CMB are well measured [102–104] and restricts h_2 lifetime $\tau_{h_2} \lesssim 1 \text{ sec}$ [105, 106]. The h_2 decay life time in our case turns,

$$\tau_{h_2} = [\Gamma_{h_2 \rightarrow \text{SM SM}} + \Gamma_{h_2 \rightarrow X X} + \Gamma_{h_2 \rightarrow \phi \phi}]^{-1}. \quad (2.17)$$

Equivalently, the total decay width of h_2 (Γ_{h_2}) should be greater than $6.58 \times 10^{-25} \text{ GeV}$, which puts a stringent limit on the model parameters. For other relevant constraints for the light scalar h_2 in presence of VBDM see [107]. Also, you may visit ref. [108, 109] for relevant bounds on light scalar DM from LEP, LHC, light meson decay, and fixed target experiments. For h_2 to remain in chemical equilibrium with thermal bath, the interaction rate of h_2 must be larger than the Hubble expansion rate,

$$\sum_{\mathcal{F}} \left[\langle \Gamma \rangle_{h_2 \rightarrow \mathcal{F} \mathcal{F}} + n_{h_2}^{\text{eq}} \langle \sigma v \rangle_{h_2 h_2 \rightarrow \mathcal{F} \mathcal{F}} \right]_{T_{\text{FO}}^{\text{DM}}} \gtrsim H(T_{\text{FO}}^{\text{DM}}), \quad (2.18)$$

where $\mathcal{F} \in \{\text{SM particles}, \phi, X\}$, and $T_{\text{FO}}^{\text{DM}} \sim m_{\text{DM}}/25$. In fig. 5, see the the variation of interaction rate of h_2 with the bath temperature. However, the kinematic equilibrium of h_2 is maintained by the inelastic scattering with light SM fermions ($h_2 \mathcal{F} \rightarrow h_2 \mathcal{F}$), sharing the same SM bath temperature (T), so that we use $n_{h_2}(T) \simeq n_{h_2,0}(T)$ throughout the analysis; one can also study the departure from the aforementioned condition via solving the three coupled Boltzmann equations (cBEQ) simultaneously.

• Limits on thermal dark matter annihilation

CMB anisotropies constrain energy injection from DM annihilation, providing limits on WIMP annihilation cross-sections that complement indirect DM searches. Planck 2018

data constrains DM mass and annihilation cross-section; the strongest bounds are obtained assuming s-wave annihilation into bottom quark pairs, $\langle\sigma v\rangle_{\text{DM DM}\rightarrow b\bar{b}} \sim 8 \times 10^{-27} \text{ cm}^3/\text{s}$ for $m_{\text{DM}} = 6 \text{ GeV}$ [1]. On the other hand, the 95% confidence level upper limits on the thermally-averaged cross-section for DM particles annihilating into $b\bar{b}$, derived from a combined analysis of 158 hours of Segue 1 observation with MAGIC, and 6-year observations of 15 dwarf satellite galaxies by the Fermi-LAT, is $\sim 10^{-26} \text{ cm}^3/\text{s}$ for $m_{\text{DM}} = 6 \text{ GeV}$ [110].

3 Coupled Boltzmann Equation and Relic density

In this study, we have considered both the dark sector particles as WIMP-like DM, so that both components can be probed in future DD experiments. In particular, we are interested in the possibility of getting a kink in the recoil energy spectrum. But before that, we will address the possibility of the DM components to acquire correct relic density. WIMPs are initially in thermal equilibrium with the bath particles and undergo freeze-out when their interaction rate falls below the Hubble expansion rate. The Feynman diagrams, which provide the annihilation of DMs and DM-DM conversion processes, are shown in fig. 4. The freeze out of DM components are evaluated by solving the coupled Boltzmann Equations (cBEQs), which in our case, reads:

$$\begin{aligned} \frac{dY_\phi}{dx} &= -\frac{\mathbf{s}}{x H(x)} \left[\left(Y_\phi^2 - Y_{\phi,0}^2 \right) \langle\sigma v\rangle_{\phi\phi\rightarrow\text{SM SM}} + \left(Y_\phi^2 - Y_X^2 \frac{Y_{\phi,0}^2}{Y_{X,0}^2} \right) \langle\sigma v\rangle_{\phi\phi\rightarrow X X} \right], \\ \frac{dY_X}{dx} &= -\frac{\mathbf{s}}{x H(x)} \left[\left(Y_X^2 - Y_{X,0}^2 \right) \langle\sigma v\rangle_{XX\rightarrow\text{SM SM}} + \left(Y_X^2 - Y_\phi^2 \frac{Y_{X,0}^2}{Y_{\phi,0}^2} \right) \langle\sigma v\rangle_{XX\rightarrow\phi\phi} \right] \\ &+ \frac{2}{x H(x)} \sum_{i=1}^2 \left[Y_{h_i,0} - Y_{h_i,0} \frac{Y_X^2}{Y_{X,0}^2} \right] \langle\Gamma\rangle_{h_i\rightarrow X X}. \end{aligned} \quad (3.1)$$

In the above, notations have very standard meaning, some of them worth noting are, $x = \mu_{\phi X}/T$, where $\mu_{\phi X} = m_\phi m_X/(m_\phi + m_X)$ denotes reduced mass for the two DM components, T denotes temperature of the thermal bath, $Y_{i,0} = n_{i,0}/\mathbf{s}$ denotes equilibrium yield, with $\mathbf{s} = \frac{2\pi^2}{45} g_*^s T^3$ denoting entropy density, $n_{i,0} = \frac{T}{2\pi^2} g_i m_i^2 K_2\left(\frac{m_i}{T}\right)$ indicate to equilibrium number density, annihilation final states include $\text{SM} \in \{h_1, h_2, W^\pm, Z, \text{leptons and quarks}\}$, and

$$\langle\sigma v\rangle_{a b\rightarrow c d} n_{a,0} n_{b,0} = \langle\sigma v\rangle_{c d\rightarrow a b} n_{c,0} n_{d,0}, \quad (3.2)$$

indicate the thermal average of annihilation cross-section. The total DM relic density is the sum of the individual relic densities, derived from the solution of the cBEQ in eq. 3.1, to provide,

$$\Omega_{\text{DM}} h^2 = 2.744 \times 10^8 [m_\phi Y_\phi + m_X Y_X]_{x\rightarrow\infty}. \quad (3.3)$$

The free parameters in this model that crucially dictates DM phenomenology are,

$$\{m_\phi, m_X, m_{h_2}, g_X, \lambda_{\phi H}, \lambda_{\phi S}, \sin\vartheta\}. \quad (3.4)$$

The parameter space which is scanned here is : $\{10^{-3} < \lambda_{\phi S} < 1, 10^{-4} < \lambda_{\phi H} < 10^{-1}, 10^{-3} < g_X < 10^{-1}, 10^{-4} < |\sin \vartheta| < 10^{-2}, 1 < m_X < 550, 1 < m_{h_2} < 10^3, 1 < m_\phi < 10^3\}$ where masses are in GeV unit. We have calculated the DM relic densities and the spin-independent (SI) DM-nucleon inelastic scattering cross-section using MicrOMEGAs 6.0 [111], and the findings are presented and discussed below.

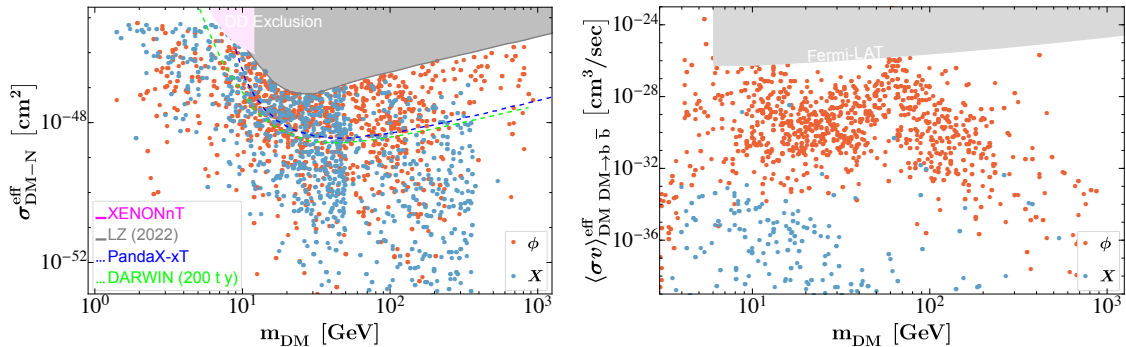


Figure 1: *Left:* Allowed parameter space of the model in the $m_{\text{DM}} - \sigma_{\text{DM-N}}^{\text{eff}}$ plane (ϕ in blue, X in red points) that satisfies $\mathcal{B}_{h_1 \rightarrow \text{inv}} \leq 0.113$ and $\tau_{h_2} < 1$ sec, relic abundance and indirect search (DM DM \rightarrow b $\bar{\text{b}}$) constraints from Fermi-LAT and CMB. The bounds and future sensitivities from experiments like XENONnT, LZ, PandaX-xT, DARWIN are shown. *Right:* points allowed by relic density, and recent direct detection constraint from LZ-2022 in $m_{\text{DM}} - \langle \sigma v \rangle_{\text{DM DM} \rightarrow \text{b} \bar{\text{b}}}^{\text{eff}}$ plane are shown with Fermi-LAT bound.

In the left plot of fig. 1, we illustrate the relic density allowed points in the $m_{\text{DM}} - \sigma_{\text{DM-N}}^{\text{eff}}$ plane. The orange points represent real scalar DM (ϕ), while the light blue points correspond to VBDM (X). The effective SI DM-nucleon scattering cross-section is defined as $\sigma_{iN}^{\text{eff}} = (\Omega_i/\Omega_{\text{tot}})\sigma_{iN}^{\text{SI}}$, where the individual direct search cross-section is scaled by the ratio of its relative abundance with respect to the total one. The grey (LZ-2022 [112]) and pink (XENONnT [113]) shaded regions indicate the DD exclusion limits, while the projected limits are shown by the dashed blue (PandaX-xT [114]) and green (DARWIN-200 t y [115, 116]) lines. The points scanned here already obey indirect detection and collider search limits. Additionally, two peaks in the indirect detection signal $\langle \sigma v \rangle_{\text{DM DM} \rightarrow \text{b} \bar{\text{b}}}$ occur near the h_1 and h_2 resonances, leading to the exclusion of some points in these regions. The major stumble block in coming up with a realistic model that produces a curvature in the direct search signal is that one of the DM components must have small mass, therefore susceptible to the invisible branching ratio of either the Higgs or Z boson or whatever the DM-SM portal is. In our case, we need to adhere to the Higgs invisible decay bound, and we can address that by choosing a very small mixing angle $|\sin \vartheta| \lesssim 10^{-2}$. This was one of the reasons of having the second light scalar present in the scenario. From the figure, it is clear that there is plenty of breathing space for the model to survive the non-observation of direct search limit after addressing the observed relic density, with both the DM components providing detectable points in the vicinity of the exclusion limit and beyond. Notably, we are considering spin independent direct search cross-section and the corresponding limits as obtained by the DM interactions in this model.

In the right plot in fig. 1, we have shown the relic density allowed points in $m_{\text{DM}} -$

$\langle\sigma v\rangle_{\text{DM DM}\rightarrow\text{b}\bar{\text{b}}}^{\text{eff}}$ plane, where the colour coding remains the same as the left plot. All the points shown here are also allowed by direct and collider search constraints. This particular annihilation channel to the bottom quark pair is relevant as some points are excluded near the Higgs resonance region from the Fermi-LAT [36, 37, 117] limit. There are points below the Higgs mass, which also get restricted because of the resonance enhancement due to the presence of the light mediator h_2 .

4 Two component dark matter signal in direct detection

After finding out the allowed parameter space of the model from the existing bounds, we now turn to the direct search observability of two DM components. Its worth repeating that we wish to focus on the direct search signal where a kink or a curvature in the recoil energy spectrum is observed [56, 57]. Absent any background, this indicates the presence of more than one DM components. In the context of the model presented above, it is therefore the exploration of the region of parameter space where the presence of two DM components can be realised.

Let us now turn to the formalism a little. The total observed differential event rate is the sum of the individual event rates from each DM component interacting with the target nuclei. The DM relic densities as obtained from the solution of cBEQ are given by,

$$\Omega_X h^2 = \frac{\rho_X}{\rho_{\text{crit}}}, \quad \Omega_\phi h^2 = \frac{\rho_\phi}{\rho_{\text{crit}}}, \quad \text{with} \quad \rho_{\text{loc}} = \rho_X + \rho_\phi, \quad (4.1)$$

where the critical density is given by $\rho_{\text{crit}} = \frac{3H_0^2}{8\pi G} \sim$, with H_0 and G representing the Hubble and gravitational constants respectively. Following the above relations, we can evaluate the DM densities in terms of relic densities,

$$\rho_\phi = \rho_{\text{loc}} \frac{\Omega_\phi h^2}{\Omega_\phi h^2 + \Omega_X h^2}, \quad \text{and} \quad \rho_X = \rho_{\text{loc}} \frac{\Omega_X h^2}{\Omega_\phi h^2 + \Omega_X h^2}, \quad (4.2)$$

and

$$\rho_\phi \sigma_\phi^N = \rho_{\text{loc}} \frac{\Omega_\phi h^2}{\Omega_\phi h^2 + \Omega_X h^2} \sigma_\phi^N \equiv \rho_{\text{loc}} \sigma_{\phi-N}^{\text{eff}}, \quad \text{and} \quad \rho_X \sigma_X^N = \rho_{\text{loc}} \sigma_{X-N}^{\text{eff}}. \quad (4.3)$$

The time-averaged event rate for recoil, typically measured in events/(kg keV day), for a detector with a target nucleus³ of mass m_A and characterized by the standard notation (A, Z) , is given by the sum of the individual contributions,

$$R_A(E_R) = R_A^{(1)}(E_R) + R_A^{(2)}(E_R) = F_A^2(E_R) \sum_{\alpha=X,\phi} (A_\alpha^{\text{eff}})^2 \frac{\rho_\alpha \sigma_\alpha^p}{2m_\alpha \mu_{\alpha p}} \eta_\alpha(v_m^\alpha, m_A, t), \quad (4.4)$$

³In this article, we have considered the $^{132}\text{Xe}_{54}$ as our detector nuclei. However, we can do a similar analysis for other nuclei such as germanium (EDELWEISS [50]) and sodium (COSINE-100 [118]) for the spin independent case, while fluorine (PICO [119]) for the spin-dependent case, etc.

where the nuclear form factor of the detector element with the mass number A is denoted by $F_A(E_R)$, where E_R denotes recoil energy. For the spin independent (SI) form factor, we use the Helm parametrization [120, 121]. The velocity integral ($\eta_\alpha(v_m^\alpha, m_A, t)$) is defined as,

$$\eta_\alpha(v_m^\alpha, m_A, t) = \int_{v_{m,A}^{(\alpha)}} d^3v \frac{f_{\text{det}}^{(\alpha)}(\mathbf{v}, t)}{v}, \quad (4.5)$$

where $v_{m,A}^{(\alpha)} = \sqrt{\frac{m_A E_R}{2\mu_{\alpha A}^2}}$ is the minimum velocity required for a DM particle α to produce a nuclear recoil with energy E_R (the detector's threshold) in a nucleus of mass m_A . The velocity distribution of DM particles in the detector frame, $f_{\text{det}}^{(\alpha)}(\mathbf{v}, t)$, satisfies $f_{\text{det}}^{(\alpha)}(\mathbf{v}, t) \geq 0$ and $\int f_{\text{det}}^{(\alpha)}(\mathbf{v}, t) d^3v = 1$. The velocity distributions in the detector and galaxy rest frames are related further by a Galilean transformation: $f_{\text{det}}(\mathbf{v}, t) = f_{\text{gal}}(\mathbf{v} + \mathbf{v}_e(t))$, where $\mathbf{v}_e(t)$ is the Earth's velocity in the galaxy's rest frame. Here, we have used the Standard Halo Model, assuming a local DM density of $\rho_{\text{loc}} \simeq 0.4 \text{ GeV/cm}^3$ and a Maxwellian velocity distribution [122–124],

$$f_{\text{gal}}(v) = \frac{1}{(2\pi v_\alpha^2)^{3/2}} \exp\left(-\frac{3}{2} \frac{v^2}{v_\alpha^2}\right), \quad (4.6)$$

with a cutoff at the escape velocity, $v_{\text{esc}} = 550 \text{ km s}^{-1}$ [125, 126]. The velocity dispersion v_α depend on the DM masses within the model following,

$$v_\alpha = v_0 (\bar{m}/m_\alpha)^{1/2}, \quad (4.7)$$

where the canonical value for the velocity dispersion is $v_0 \sim 270 \text{ km s}^{-1}$ [127, 128], and

$$\bar{m} = \frac{\sum_{k=1,2} n_k m_k / \sum_{l=1,2} n_l}{\sum_{k=1,2} \Omega_k h^2} = \frac{\rho_{\text{loc}} / (n_1 + n_2)}{\left(\sum_{l=1,2} \frac{\Omega_l h^2}{m_l}\right)^{-1}}. \quad (4.8)$$

The scattering cross-section of DM particle α with the protons at zero momentum transfer is denoted by σ_α^p , while $\mu_{\alpha p}$ represents the reduced mass of the DM particle α and the proton. The nuclear form factor of the nucleus j is denoted by $F_j(E_R)$. The effective mass number of nucleus j , interacting with the DM particle α , is $A_\alpha^{\text{eff}} = Z + (A - Z)f_\alpha^n/f_\alpha^p$ with $f_\alpha^{n,p}$ representing the SI coupling strengths of the DM particle α to neutrons and protons respectively. For the SI form factors, we use the Helm parametrization in our numerical analysis [120, 121].

In tab. 2, we present several benchmark points that account for the current DM relic density, stringent direct detection limits from LZ (2022), indirect detection constraints on DM annihilation into bottom quarks, and collider limits on the Higgs invisible decay. We also have accounted for the limits on the mixing angle $\sin\vartheta$ and the BBN limit on the h_2 lifetime. Each benchmark, labeled A to G, shows a noticeable kink in the recoil energy spectrum following the methodology described above. The variation of the total

Benchmarks	m_ϕ [GeV]	m_X [GeV]	$\Omega_\phi h^2$	$\Omega_X h^2$	$\sigma_{\phi-N}^{\text{eff}}$ [cm ²]	$\sigma_{X-N}^{\text{eff}}$ [cm ²]
A	109.65	8.77	0.0352	0.0851	2.00×10^{-47}	1.98×10^{-47}
B	77.17	12.16	0.0264	0.0934	5.38×10^{-49}	2.06×10^{-48}
C	66.07	12.42	0.0005	0.11902	4.99×10^{-48}	1.91×10^{-47}
D	51.29	8.42	2.8×10^{-5}	0.1202	3.95×10^{-49}	4.55×10^{-48}
E	40.74	8.46	2.4×10^{-5}	0.1208	1.18×10^{-48}	2.09×10^{-47}
F	199.53	13.18	0.0379	0.0822	3.23×10^{-48}	4.41×10^{-48}
G	83.18	4.27	0.0294	0.0915	1.10×10^{-47}	1.10×10^{-47}

Table 2: The benchmark points noted above are capable of displaying a noticeable kink in the recoil rate spectrum while also meeting the constraints from relic density, DD, ID, and collider searches of DM.

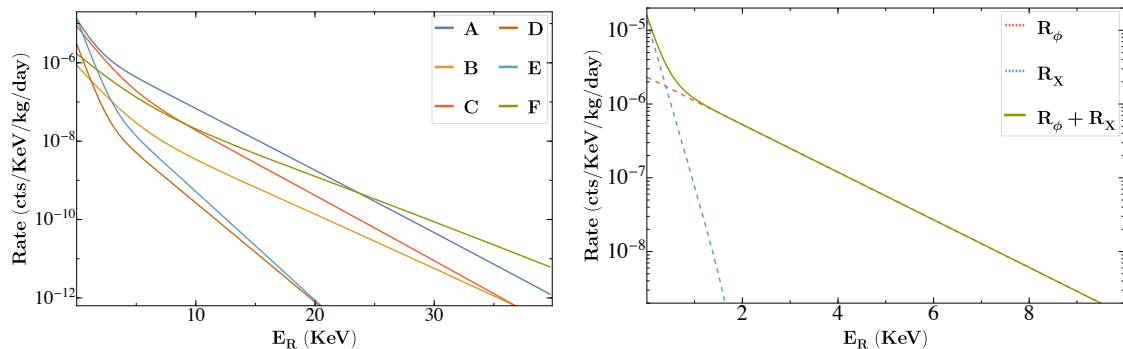


Figure 2: Recoil rate spectrum for the benchmark points as in table 2. We show the variation of total event rate ($R_\phi + R_X$) with the recoil energy (E_R). The right plot shows benchmark G, while the left plot demonstrates benchmark points A to F from table 2. The dashed blue and orange lines on the right panel correspond to the individual rates from vector boson and real scalar DM respectively.

time-averaged event rate as a function of recoil energy (E_R) is shown in fig. 2. All the benchmark points described in table 2 are shown here by different coloured lines. The kink typically appears around $E_R \lesssim 10$ keV. Its position depends not only on the DM mass but also on the relic density and the SI DM-nucleon scattering cross-section. In the left panel, E_R ranges up to 40 keV, while in the right panel, it is limited to 10 keV for a closer inspection of the kink. We also show on the right panel, how the different slopes in R_ϕ and R_X adds to the kink. It is obvious that there are regions of parameter space, where the slope for both DM components are same in the recoil spectrum, where the distinguishability is submerged. So it is legitimate to ask, what is the parameter that crucially governs the kink. The answer to that is DM mass. So, the larger the mass is, the smaller the slope

is. Whenever, there is a substantial gap in the slope between the DM components, having similar direct search cross-section, such distinctive curvature will appear to indicate the presence of two DM components.

The angles between the linear fit of the vector and scalar DM event rate curves, measured from the positive E_R axis, are represented as θ_X and θ_ϕ , respectively. The resultant angle between these two curves is defined as $\theta = \theta_X - \theta_\phi$. If $m_X > m_\phi$, then $\theta_\phi < \theta_X$, resulting in a positive angle. Conversely, if $m_X < m_\phi$, then $\theta_\phi > \theta_X$, yielding a negative angle. However, other parameters, such as DM relic density and DD cross-section, can influence the slope, though their effects are mild and flexible, with a considerable impact on event rates.

Finally, in fig. 3, we show the points in the $m_\phi - m_X$ plane that satisfy the DM relic density and respect the DD, ID, and collider constraints. Importantly, the rainbow color bar represents the angle (θ , in degrees) between the two linear fit lines for the event rates of the two DM particles, X and ϕ in the recoil energy spectrum. We see the presence of bluish or yellow-reddish points, where the angle is large to make the kink visible, spanning at large m_ϕ with small m_X . This also validates the claim made in model independent way in the references [56, 57] that the kink appears only when one mass is around 10 GeV, and the other is $\gtrsim 40$ GeV. On the contrary, for the opposite mass hierarchy, i.e. $m_X > m_\phi$, energy densities are widely different with $\rho_\phi \ll \rho_X$, and the event rates for ϕ is way smaller as $R_\phi \ll R_X$ across the entire range of E_R . Consequently, this hierarchy is less promising for discriminating between the two DM components, although a finite slope difference exists between the two linear-fitted event rate curves. However, the situation alters if we can have $\rho_\phi > \rho_X$ for $m_\phi < m_X$ by incorporating new degrees of freedom into our model. Thus, our work provides an example of a UV-complete vector-scalar model, where the distinguishability in direct search could be demonstrated. This is possible due to the presence of light scalar (h_2), which helps keep the VBDM under relic, even below the Higgs resonance. We also note that as a result, the benchmark points where VBDM is light, provides the majority of the relic density contribution. However, the possibility of having equal share of relic density is difficult, at least in this model, to provide a distinctive direct search signal for the presence of both.

A statistical method using frequentist statistics for assessing the sensitivity of future experiments to distinguish between a single- and two-component DM scenario was discussed in detail by [56]. It involves hypothesis testing and parameter estimation, where DM masses, the DM-nucleon scattering cross-section, and the energy density of each component and the same velocity dispersion assuming SHM are assumed free. In contrast, these parameters excepting for the DM mass are evaluated in our model following their interactions, adhering to all observation constraints.

5 Summary and conclusions

There are many possibilities embedded in multi-component DM, both in construction and phenomenology. The limits on the self-interaction of DM from the galaxy cluster observations like Bullet, Abell clusters does not clarify the ambiguity of its component type, as

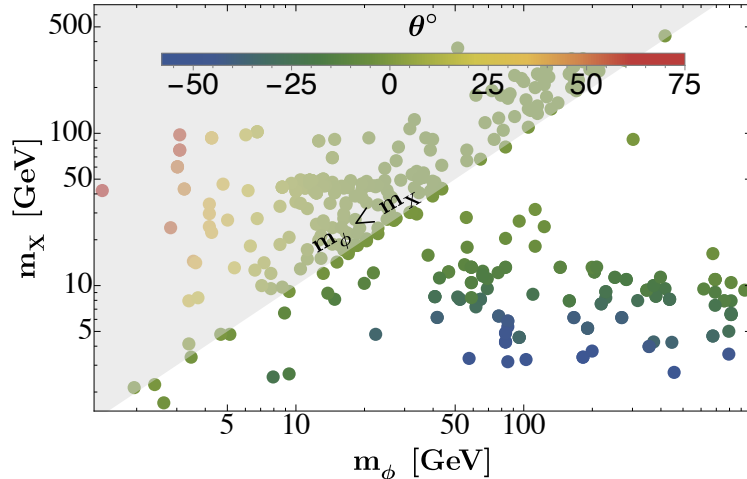


Figure 3: Rainbow color bar shows the variation of angle between the two event rate lines w.r.t E_R , while the θ is in degree. The grey-shaded region is insensitive for experiments to discriminate the slope due to the difference in even rates, although accommodates large θ ; for details, see the main text.

the self-interaction could be among the same or different kinds of particles that constitute the 26.8% dark sector of the observed universe. An extended dark sector provides different phenomenological advantages specifically due to the DM-DM conversion, however an observational signal can only testify such hypothesis. Therefore, observation of two component DM signals in direct detection (DD), indirect detection (ID), and collider experiments are important to study. In this article, we have focused on multi-component DM signals in direct detection experiments.

In model independent analysis [56, 57], it was argued that a kink in the nuclear recoil rate can provide such a useful hint of having two different DMs coexisting and producing direct search signal. However, we don't know of an analysis where a UV complete model was studied to discuss such possibilities. Now, this is important as several constraints both from theoretical consistency as well as from observations like collider searches, indirect searches limit such models heavily with a potential possibility that the region of the parameter space where such distinguishability is observed, is actually discarded. This was the main point of concern and rationale behind our study. Many of the simple kind of two component DM models studied so far fails to provide such distinguishability, where the model is valid, like having two scalar/fermion singlets; one singlet, one doublet etc.

In the proposed model, we extend the SM by introducing a SM gauge-singlet real scalar (ϕ) stable under \mathcal{Z}'_2 and a complex scalar S respecting $U(1)_X$ gauge symmetry. The associated gauge boson X , stable under \mathcal{Z}_2 , serves as the second DM candidate. The singlet-doublet mixing generates a new scalar (h_2) together with the SM Higgs (h_1). The mixing angle (ϑ) serves as a crucial variable, that can make one DM light, after addressing Higgs invisible decay and (in)direct detection of DMs, by choosing $|\sin \vartheta| \lesssim 10^{-2}$. The individual relic densities are calculated by solving the cBEQ. We assume the light scalar h_2 to be in thermal bath, the rationale of which is explained in Appendix B. Another

strong constraint comes from the BBN, as the presence of a light scalar can alter the BBN prediction of the Λ CDM model. Therefore, the lifetime of this light scalar should be smaller than 1 sec. Further, for direct and indirect detection, we calculate the ‘effective’ DM-nucleon scattering and annihilation cross-sections, as they most often contribute to total relic density unequally.

Further, we calculate the time-averaged event rate, assuming that both DMs scatter off the detector nuclei and making it recoil. We plot the time-averaged event rate with the recoil energy for several benchmark points, respecting all relevant constraints to show that a kink in the recoil rate can be observed. The event rate depends not only on DM masses, DM number densities, DM-nucleon scattering cross-section, but also on the detector materials, and their sensitivity decides the minimum recoil energy required to produce detectable signals. Our analysis is based mainly on $^{132}\text{Xe}_{54}$ material used in LZ, XENON, PandaX, and the threshold recoil energy for nuclear recoil events is 1 KeV as used for XENONnT experiments. The curvature of the resultant event rate spectrum, which is the summation of event rates corresponding to the two DMs, provides the proof of the existence of more than one DM. Here, we measure the curvature by measuring the angle between two asymptotic lines corresponding to the event rates of two DMs. The position of the resultant kink depends upon several parameters, like DM mass, relative abundances, DM-nucleon scattering cross-section etc. The observability of the kink, or what is the minimum angle (θ_{\min}) below which we are unable to differentiate between single-component and two-component DM frameworks is another question. This is discussed partly via statistical analysis in [56]. According to our model, the maximum achieved angle is $\sim 75^\circ$, where $m_\phi \lesssim 5$ GeV and $m_X \gtrsim 40$ GeV, and $\sim -60^\circ$, where $m_X \lesssim 5$ GeV and $m_\phi \gtrsim 40$ GeV. However, for $m_X > m_\phi$, the energy densities are highly different, $\rho_\phi \ll \rho_X$, and the event rates for ϕ is way smaller than X , as $R_\phi \ll R_X$ across the entire range of E_R , thus making the observability of the kink in the recoil rate nearly impossible.

Therefore, the requirement that the recoil rates can’t differ too much for the DM components by having DM-nucleon cross-section at the same ballpark, but the slope in recoil rate requires to be different by having different DM masses, favours a specific mass hierarchy $m_X < m_\phi$ for our model to show the kink. The difference in DM mass results in different relic density contributions. Such a conclusion was not possible to draw from a model independent analysis. Further, the possibility of having a kink in the direct search signal together with that of a double bump signal in the collider is an interesting question, or of their complementarity, if exists, which we plan to study later.

Acknowledgement: SB would like to acknowledge Grant No. CRG/2019/004078 from SERB, Govt. of India. Although the tenure of the project has ended now, we started looking into such possibilities, as part of the project deliverables.

A Feynman diagrams for DM relic density

In the two component DM model, constructed of a VBDM (X) and a scalar singlet (ϕ) in thermal bath as described in Section . 2, their annihilation cross-sections to the SM particles

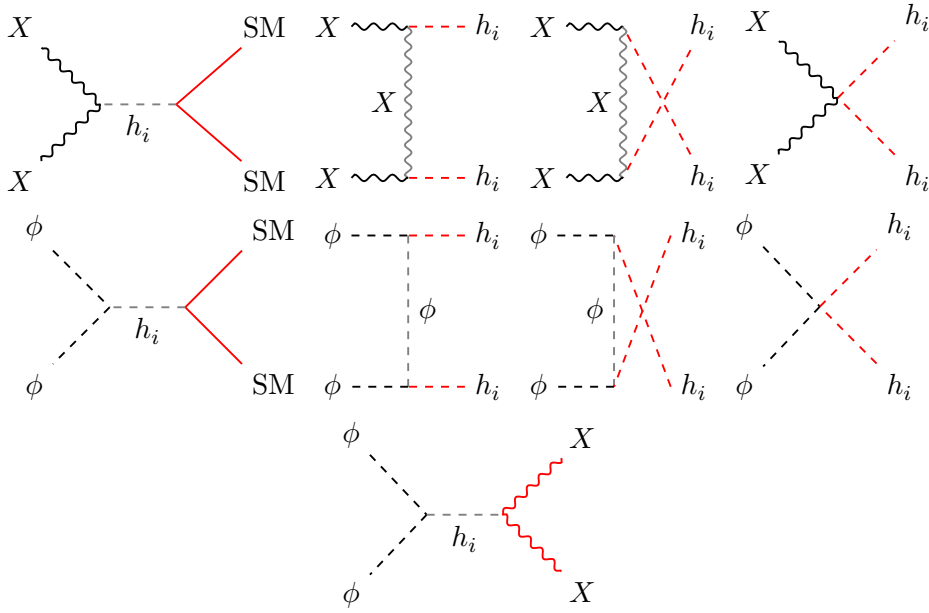


Figure 4: Feynman diagrams relevant for DM annihilation: $\phi\phi \rightarrow \text{SM SM}$ and $X X \rightarrow \text{SM SM}$, where $\text{SM} \in \{h_i, \text{quarks, leptons, } W^\pm, Z\}$, and $i = 1, 2$. The bottom panel Feynman diagram shows the DM-DM conversion: $\phi\phi \rightarrow X X$.

and conversion amongst themselves crucially decide the relic densities of the individual components. The Feynman graphs are shown in fig. 4. The individual relic densities also dictate the effective direct and indirect search cross-sections.

B Thermal equilibrium for h_2

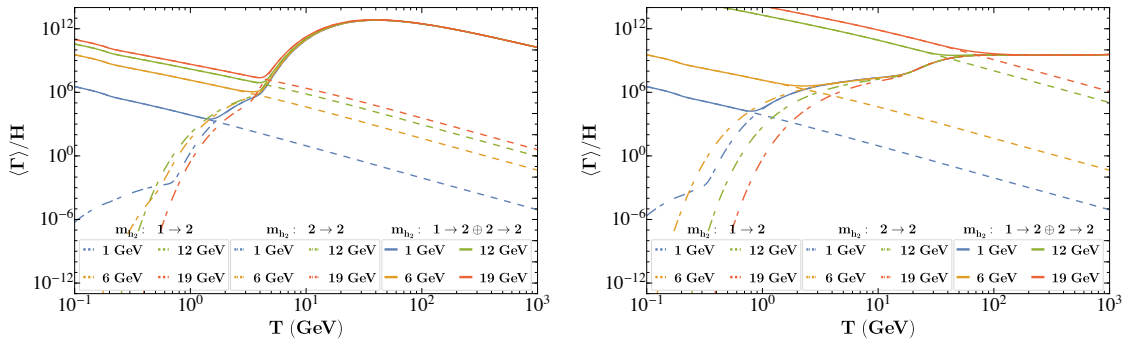


Figure 5: $\langle \Gamma \rangle / H$ versus bath temperature T plotted for h_2 . The dashed, dot-dashed, and thick color lines show the interaction rate of h_2 for decay, scattering, and the combined decay plus scattering processes, respectively. The parameters kept constant are: $g_X = 10^{-2}$, $\sin \vartheta = 10^{-3}$, $\lambda_{\phi S} = 10^{-1}$, $\lambda_{\phi H} = 10^{-2}$, while for left : $\{m_\phi = 50 \text{ GeV, and } m_X = 10 \text{ GeV}\}$, and for right : $\{m_\phi = 100 \text{ GeV, and, } m_X = 5 \text{ GeV}\}$, with four distinct colors representing different values of m_{h_2} .

The key assumption in solving the cBEQ for obtaining ϕ and X relic densities, is that during DM freeze-out, h_2 remains in chemical and kinetic equilibrium, i.e., $n_{h_2}(T) =$

$n_{h_2,0}(T)$, and shares the same thermal bath temperature. The kinetic and chemical equilibria are maintained via scattering with relativistic SM fermions and annihilation and decay to the light SM fermions, respectively. The results are shown in fig. 5, where $\langle\Gamma\rangle/H$ is plotted against bath temperature (T) for some allowed parameters of the model to show that in all cases including decay and scattering, h_2 remains in thermal bath.

References

- [1] PLANCK collaboration, *Planck 2018 results. VI. Cosmological parameters*, *Astron. Astrophys.* **641** (2020) A6 [1807.06209].
- [2] G. Bertone, D. Hooper and J. Silk, *Particle dark matter: Evidence, candidates and constraints*, *Phys. Rept.* **405** (2005) 279 [hep-ph/0404175].
- [3] J.M. Cline, K. Kainulainen, P. Scott and C. Weniger, *Update on scalar singlet dark matter*, *Phys. Rev. D* **88** (2013) 055025 [1306.4710].
- [4] L. Roszkowski, E.M. Sessolo and S. Trojanowski, *WIMP dark matter candidates and searches—current status and future prospects*, *Rept. Prog. Phys.* **81** (2018) 066201 [1707.06277].
- [5] B.W. Lee and S. Weinberg, *Cosmological Lower Bound on Heavy Neutrino Masses*, *Phys. Rev. Lett.* **39** (1977) 165.
- [6] P. Gondolo and G. Gelmini, *Cosmic abundances of stable particles: Improved analysis*, *Nucl. Phys. B* **360** (1991) 145.
- [7] Y. Hochberg, E. Kuflik, T. Volansky and J.G. Wacker, *Mechanism for Thermal Relic Dark Matter of Strongly Interacting Massive Particles*, *Phys. Rev. Lett.* **113** (2014) 171301 [1402.5143].
- [8] L.J. Hall, K. Jedamzik, J. March-Russell and S.M. West, *Freeze-In Production of FIMP Dark Matter*, *JHEP* **03** (2010) 080 [0911.1120].
- [9] D. Clowe, A. Gonzalez and M. Markevitch, *Weak lensing mass reconstruction of the interacting cluster 1E0657-558: Direct evidence for the existence of dark matter*, *Astrophys. J.* **604** (2004) 596 [astro-ph/0312273].
- [10] M. Markevitch, A.H. Gonzalez, D. Clowe, A. Vikhlinin, L. David, W. Forman et al., *Direct constraints on the dark matter self-interaction cross-section from the merging galaxy cluster 1E0657-56*, *Astrophys. J.* **606** (2004) 819 [astro-ph/0309303].
- [11] S.W. Randall, M. Markevitch, D. Clowe, A.H. Gonzalez and M. Bradac, *Constraints on the Self-Interaction Cross-Section of Dark Matter from Numerical Simulations of the Merging Galaxy Cluster 1E 0657-56*, *Astrophys. J.* **679** (2008) 1173 [0704.0261].
- [12] F. Kahlhoefer, K. Schmidt-Hoberg, J. Kummer and S. Sarkar, *On the interpretation of dark matter self-interactions in Abell 3827*, *Mon. Not. Roy. Astron. Soc.* **452** (2015) L54 [1504.06576].
- [13] J. Merten, D. Coe, R. Dupke, R. Massey, A. Zitrin, E.S. Cypriano et al., *Creation of cosmic structure in the complex galaxy cluster merger Abell 2744*, *Monthly Notices of the Royal Astronomical Society* **417** (2011) 333 [<https://academic.oup.com/mnras/article-pdf/417/1/333/3023087/mnras0417-0333.pdf>].
- [14] S. Profumo, K. Sigurdson and L. Ubaldi, *Can we discover multi-component WIMP dark matter?*, *JCAP* **12** (2009) 016 [0907.4374].
- [15] S. Bhattacharya, A. Drozd, B. Grzadkowski and J. Wudka, *Two-Component Dark Matter*, *JHEP* **10** (2013) 158 [1309.2986].
- [16] A. Dutta Banik, M. Pandey, D. Majumdar and A. Biswas, *Two component WIMP-FIMP dark matter model with singlet fermion, scalar and pseudo scalar*, *Eur. Phys. J. C* **77** (2017) 657 [1612.08621].

- [17] M. Pandey, D. Majumdar and K.P. Modak, *Two Component Feebly Interacting Massive Particle (FIMP) Dark Matter*, *JCAP* **06** (2018) 023 [[1709.05955](#)].
- [18] S. Peyman Zakeri, S. Mohammad Moosavi Nejad, M. Zakeri and S. Yaser Ayazi, *A Minimal Model For Two-Component FIMP Dark Matter: A Basic Search*, *Chin. Phys. C* **42** (2018) 073101 [[1801.09115](#)].
- [19] S.-Y. Ho, P. Ko and C.-T. Lu, *Scalar and fermion two-component SIMP dark matter with an accidental \mathbb{Z}_4 symmetry*, *JHEP* **03** (2022) 005 [[2201.06856](#)].
- [20] S.-M. Choi, J. Kim, P. Ko and J. Li, *A multi-component SIMP model with $U(1)_X \rightarrow \mathbb{Z}_2 \times \mathbb{Z}_3$* , *JHEP* **09** (2021) 028 [[2103.05956](#)].
- [21] S. Bhattacharya, J. Lahiri and D. Pradhan, *Detection possibility of a Pseudo-FIMP in presence of a thermal WIMP*, [2212.14846](#).
- [22] S. Bhattacharya, J. Lahiri and D. Pradhan, *Dynamics of the pseudo-FIMP in presence of a thermal Dark Matter*, [2212.07622](#).
- [23] S. Bhattacharya, L. Kolay and D. Pradhan, *Multiparticle scalar dark matter with \mathbb{Z}_N symmetry*, [2410.16275](#).
- [24] J. Lahiri, D. Pradhan and A. Sarkar, *The Influence of Lepton Portal on the WIMP-pFIMP framework*, [2410.19734](#).
- [25] S. Bhattacharya, D. Pradhan and J. Thakkar., *Pseudo-FIMP dark matter in presence of a SIMP*, [2411.15108](#).
- [26] I. Zurbano Fernandez et al., *High-Luminosity Large Hadron Collider (HL-LHC): Technical design report*, .
- [27] FCC collaboration, *Towards Future Circular Colliders*, *PoS LHCP2018* (2018) 268.
- [28] CEPC STUDY GROUP collaboration, *CEPC Technical Design Report: Accelerator*, *Radiat. Detect. Technol. Methods* **8** (2024) 1 [[2312.14363](#)].
- [29] C. Accettura et al., *Towards a muon collider*, *Eur. Phys. J. C* **83** (2023) 864 [[2303.08533](#)].
- [30] P. Bambade et al., *The International Linear Collider: A Global Project*, [1903.01629](#).
- [31] O. Buchmueller, C. Doglioni and L.T. Wang, *Search for dark matter at colliders*, *Nature Phys.* **13** (2017) 217 [[1912.12739](#)].
- [32] CDF, D0 collaboration, *Updated Combination of CDF and D0 Searches for Standard Model Higgs Boson Production with up to 10.0 fb^{-1} of Data*, 7, 2012 [[1207.0449](#)].
- [33] LEP, ALEPH, DELPHI, L3, OPAL collaboration, *Electroweak parameters of the Z^0 resonance and the Standard Model: the LEP Collaborations*, *Phys. Lett. B* **276** (1992) 247.
- [34] L. Evans and P. Bryant, eds., *Lhc machine*, *JINST* **3** (2008) S08001.
- [35] J.M. Gaskins, *A review of indirect searches for particle dark matter*, *Contemp. Phys.* **57** (2016) 496 [[1604.00014](#)].
- [36] FERMI-LAT collaboration, *Searching for Dark Matter Annihilation from Milky Way Dwarf Spheroidal Galaxies with Six Years of Fermi Large Area Telescope Data*, *Phys. Rev. Lett.* **115** (2015) 231301 [[1503.02641](#)].
- [37] FERMI-LAT collaboration, *Sensitivity Projections for Dark Matter Searches with the Fermi Large Area Telescope*, *Phys. Rept.* **636** (2016) 1 [[1605.02016](#)].

- [38] H.E.S.S. collaboration, *Search for dark matter annihilations towards the inner Galactic halo from 10 years of observations with H.E.S.S.*, *Phys. Rev. Lett.* **117** (2016) 111301 [[1607.08142](#)].
- [39] H. Silverwood, C. Weniger, P. Scott and G. Bertone, *A realistic assessment of the CTA sensitivity to dark matter annihilation*, *JCAP* **03** (2015) 055 [[1408.4131](#)].
- [40] M.W. Goodman and E. Witten, *Detectability of Certain Dark Matter Candidates*, *Phys. Rev. D* **31** (1985) 3059.
- [41] R. Essig, J. Mardon and T. Volansky, *Direct Detection of Sub-GeV Dark Matter*, *Phys. Rev. D* **85** (2012) 076007 [[1108.5383](#)].
- [42] PANDA-X, PANDAX collaboration, *PandaX-xT—A deep underground multi-ten-tonne liquid xenon observatory*, *Sci. China Phys. Mech. Astron.* **68** (2025) 221011 [[2402.03596](#)].
- [43] XENON collaboration, *First Dark Matter Search with Nuclear Recoils from the XENONnT Experiment*, *Phys. Rev. Lett.* **131** (2023) 041003 [[2303.14729](#)].
- [44] LZ COLLABORATION collaboration, *Dark Matter Search Results from 4.2 Tonne-Years of Exposure of the LUX-ZEPLIN (LZ) Experiment*, [2410.17036](#).
- [45] XLZD collaboration, *The XLZD Design Book: Towards the Next-Generation Liquid Xenon Observatory for Dark Matter and Neutrino Physics*, [2410.17137](#).
- [46] XENON collaboration, *Searching for Heavy Dark Matter near the Planck Mass with XENON1T*, *Phys. Rev. Lett.* **130** (2023) 261002 [[2304.10931](#)].
- [47] SUPERCDMS collaboration, *Light Dark Matter Search with a High-Resolution Athermal Phonon Detector Operated Above Ground*, *Phys. Rev. Lett.* **127** (2021) 061801 [[2007.14289](#)].
- [48] SUPERCDMS collaboration, *Constraints on low-mass, relic dark matter candidates from a surface-operated SuperCDMS single-charge sensitive detector*, *Phys. Rev. D* **102** (2020) 091101 [[2005.14067](#)].
- [49] SUPERCDMS collaboration, *Search for low-mass dark matter via bremsstrahlung radiation and the Migdal effect in SuperCDMS*, *Phys. Rev. D* **107** (2023) 112013 [[2302.09115](#)].
- [50] EDELWEISS collaboration, *First germanium-based constraints on sub-MeV Dark Matter with the EDELWEISS experiment*, *Phys. Rev. Lett.* **125** (2020) 141301 [[2003.01046](#)].
- [51] CRESST collaboration, *Results on sub-GeV dark matter from a 10 eV threshold CRESST-III silicon detector*, *Phys. Rev. D* **107** (2023) 122003 [[2212.12513](#)].
- [52] DARKSIDE collaboration, *Search for Dark-Matter–Nucleon Interactions via Migdal Effect with DarkSide-50*, *Phys. Rev. Lett.* **130** (2023) 101001 [[2207.11967](#)].
- [53] CDEX collaboration, *Constraints on Sub-GeV Dark Matter–Electron Scattering from the CDEX-10 Experiment*, *Phys. Rev. Lett.* **129** (2022) 221301 [[2206.04128](#)].
- [54] DAMIC-M collaboration, *Search for Daily Modulation of MeV Dark Matter Signals with DAMIC-M*, *Phys. Rev. Lett.* **132** (2024) 101006 [[2307.07251](#)].
- [55] SENSEI collaboration, *SENSEI: First Direct-Detection Results on sub-GeV Dark Matter from SENSEI at SNOLAB*, [2312.13342](#).
- [56] J. Herrero-Garcia, A. Scaffidi, M. White and A.G. Williams, *On the direct detection of multi-component dark matter: sensitivity studies and parameter estimation*, *JCAP* **11** (2017) 021 [[1709.01945](#)].

- [57] J. Herrero-Garcia, A. Scaffidi, M. White and A.G. Williams, *On the direct detection of multi-component dark matter: implications of the relic abundance*, *JCAP* **01** (2019) 008 [[1809.06881](#)].
- [58] S. Bhattacharya, P. Ghosh, J. Lahiri and B. Mukhopadhyaya, *Mono- X signal and two component dark matter: New distinction criteria*, *Phys. Rev. D* **108** (2023) L111703 [[2211.10749](#)].
- [59] S. Bhattacharya, P. Ghosh, J. Lahiri and B. Mukhopadhyaya, *Distinguishing two dark matter component particles at e^+e^- colliders*, *JHEP* **12** (2022) 049 [[2202.12097](#)].
- [60] Q.-H. Cao, E. Ma, J. Wudka and C.P. Yuan, *Multipartite dark matter*, [0711.3881](#).
- [61] ATLAS collaboration, *Combined Measurement of the Higgs Boson Mass from the $H \rightarrow \gamma\gamma$ and $H \rightarrow ZZ^* \rightarrow 4\ell$ Decay Channels with the ATLAS Detector Using $s=7, 8,$ and 13 TeV pp Collision Data*, *Phys. Rev. Lett.* **131** (2023) 251802 [[2308.04775](#)].
- [62] T. Biekötter, S. Heinemeyer and G. Weiglein, *The CMS di-photon excess at 95 GeV in view of the LHC Run 2 results*, *Phys. Lett. B* **846** (2023) 138217 [[2303.12018](#)].
- [63] S. Bhattacharya, S. Chakraborti and D. Pradhan, *Electroweak symmetry breaking and WIMP-FIMP dark matter*, *JHEP* **07** (2022) 091 [[2110.06985](#)].
- [64] J. Goldstone, A. Salam and S. Weinberg, *Broken Symmetries*, *Phys. Rev.* **127** (1962) 965.
- [65] H.B. Nielsen and S. Chadha, *On How to Count Goldstone Bosons*, *Nucl. Phys. B* **105** (1976) 445.
- [66] S.R. Coleman, *There are no Goldstone bosons in two-dimensions*, *Commun. Math. Phys.* **31** (1973) 259.
- [67] C.P. Burgess, *Goldstone and pseudoGoldstone bosons in nuclear, particle and condensed matter physics*, *Phys. Rept.* **330** (2000) 193 [[hep-th/9808176](#)].
- [68] G. Bhattacharyya and D. Das, *Scalar sector of two-Higgs-doublet models: A minireview*, *Pramana* **87** (2016) 40 [[1507.06424](#)].
- [69] J. Horejsi and M. Kladiva, *Tree-unitarity bounds for THDM Higgs masses revisited*, *Eur. Phys. J. C* **46** (2006) 81 [[hep-ph/0510154](#)].
- [70] S. Bhattacharya, P. Ghosh, A.K. Saha and A. Sil, *Two component dark matter with inert Higgs doublet: neutrino mass, high scale validity and collider searches*, *JHEP* **03** (2020) 090 [[1905.12583](#)].
- [71] K. Griest and M. Kamionkowski, *Unitarity Limits on the Mass and Radius of Dark Matter Particles*, *Phys. Rev. Lett.* **64** (1990) 615.
- [72] I. Baldes and K. Petraki, *Asymmetric thermal-relic dark matter: Sommerfeld-enhanced freeze-out, annihilation signals and unitarity bounds*, *JCAP* **09** (2017) 028 [[1703.00478](#)].
- [73] J. Smirnov and J.F. Beacom, *TeV-Scale Thermal WIMPs: Unitarity and its Consequences*, *Phys. Rev. D* **100** (2019) 043029 [[1904.11503](#)].
- [74] D. Bhatia and S. Mukhopadhyay, *Unitarity limits on thermal dark matter in (non-)standard cosmologies*, *JHEP* **03** (2021) 133 [[2010.09762](#)].
- [75] Z. Zhou, G. Liu, Y. Mu and L. Xu, *Limit on the dark matter mass from its interaction with photons*, *Phys. Rev. D* **105** (2022) 103509 [[2205.08070](#)].

- [76] G. Krnjaic and S.D. McDermott, *Implications of BBN Bounds for Cosmic Ray Upscattered Dark Matter*, *Phys. Rev. D* **101** (2020) 123022 [[1908.00007](#)].
- [77] K.M. Nollett and G. Steigman, *BBN And The CMB Constrain Light, Electromagnetically Coupled WIMPs*, *Phys. Rev. D* **89** (2014) 083508 [[1312.5725](#)].
- [78] P.F. Depta, M. Hufnagel, K. Schmidt-Hoberg and S. Wild, *BBN constraints on the annihilation of MeV-scale dark matter*, *JCAP* **04** (2019) 029 [[1901.06944](#)].
- [79] P.D. Serpico and G.G. Raffelt, *MeV-mass dark matter and primordial nucleosynthesis*, *Phys. Rev. D* **70** (2004) 043526 [[astro-ph/0403417](#)].
- [80] C.M. Ho and R.J. Scherrer, *Limits on MeV Dark Matter from the Effective Number of Neutrinos*, *Phys. Rev. D* **87** (2013) 023505 [[1208.4347](#)].
- [81] C. Boehm, M.J. Dolan and C. McCabe, *A Lower Bound on the Mass of Cold Thermal Dark Matter from Planck*, *JCAP* **08** (2013) 041 [[1303.6270](#)].
- [82] K.M. Nollett and G. Steigman, *BBN And The CMB Constrain Neutrino Coupled Light WIMPs*, *Phys. Rev. D* **91** (2015) 083505 [[1411.6005](#)].
- [83] N. Sabti, J. Alvey, M. Escudero, M. Fairbairn and D. Blas, *Refined Bounds on MeV-scale Thermal Dark Sectors from BBN and the CMB*, *JCAP* **01** (2020) 004 [[1910.01649](#)].
- [84] ATLAS collaboration, *Constraints on new phenomena via Higgs boson couplings and invisible decays with the ATLAS detector*, *JHEP* **11** (2015) 206 [[1509.00672](#)].
- [85] K. Tuominen, *Cold Particle Dark Matter*, *Symmetry* **13** (2021) 1945.
- [86] G. Chalons, D. Lopez-Val, T. Robens and T. Stefaniak, *The Higgs singlet extension at LHC Run 2*, *PoS DIS2016* (2016) 113 [[1606.07793](#)].
- [87] T. Robens and T. Stefaniak, *Status of the Higgs Singlet Extension of the Standard Model after LHC Run 1*, *Eur. Phys. J. C* **75** (2015) 104 [[1501.02234](#)].
- [88] G. Chalons, D. Lopez-Val, T. Robens and T. Stefaniak, *The Higgs singlet extension at LHC Run 2*, *PoS ICHEP2016* (2016) 1180 [[1611.03007](#)].
- [89] T.N. Robens, *Constraining extended scalar sectors at current and future colliders*, *PoS CORFU2021* (2022) 031 [[2203.17016](#)].
- [90] T. Robens, *A short overview on low mass scalars at future lepton colliders – LCWS23 proceedings*, in *International Workshop on Future Linear Colliders*, 7, 2023 [[2307.15962](#)].
- [91] S.D. Lane, I.M. Lewis and M. Sullivan, *Resonant multiscalar production in the generic complex singlet model in the multi-TeV region*, *Phys. Rev. D* **110** (2024) 055017 [[2403.18003](#)].
- [92] CMS collaboration, *Search for invisible decays of the Higgs boson produced via vector boson fusion in proton-proton collisions at $s=13$ TeV*, *Phys. Rev. D* **105** (2022) 092007 [[2201.11585](#)].
- [93] ATLAS collaboration, *Search for invisible Higgs-boson decays in events with vector-boson fusion signatures using 139 fb^{-1} of proton-proton data recorded by the ATLAS experiment*, *JHEP* **08** (2022) 104 [[2202.07953](#)].
- [94] LHC HIGGS CROSS SECTION WORKING GROUP collaboration, *Handbook of LHC Higgs Cross Sections: 4. Deciphering the Nature of the Higgs Sector*, [1610.07922](#).

- [95] CMS collaboration, *Search for a standard model-like Higgs boson in the mass range between 70 and 110 GeV in the diphoton final state in proton-proton collisions at $\sqrt{s} = 13$ TeV*, [2405.18149](#).
- [96] ATLAS collaboration, *Search for diphoton resonances in the 66 to 110 GeV mass range using 140 fb^{-1} of 13 TeV pp collisions collected with the ATLAS detector*, .
- [97] ATLAS collaboration, *Search for diphoton resonances in the 66 to 110 GeV mass range using pp collisions at $\sqrt{s} = 13$ TeV with the ATLAS detector*, [2407.07546](#).
- [98] T. Biekötter, S. Heinemeyer and G. Weiglein, *95.4 GeV diphoton excess at ATLAS and CMS*, *Phys. Rev. D* **109** (2024) 035005 [[2306.03889](#)].
- [99] S. Yaser Ayazi, M. Hosseini, S. Paktinat Mehdiabadi and R. Rouzbehi, *Vector dark matter and LHC constraints, including a 95 GeV light Higgs boson*, *Phys. Rev. D* **110** (2024) 055004 [[2405.01132](#)].
- [100] S. Gao, S.-M. Zhao, L. Ruan, X.-X. Dong and T.-F. Feng, *A 95 GeV Higgs Boson in the $U(1)_X$ model*, [2411.13261](#).
- [101] P. Janot, *The infamous 95 GeV $b\bar{b}$ excess at LEP: two b or not two b?*, *JHEP* **10** (2024) 223 [[2407.10948](#)].
- [102] G. Steigman, *Neutrinos And Big Bang Nucleosynthesis*, *Adv. High Energy Phys.* **2012** (2012) 268321 [[1208.0032](#)].
- [103] M. Kaplinghat, S. Tulin and H.-B. Yu, *Direct Detection Portals for Self-interacting Dark Matter*, *Phys. Rev. D* **89** (2014) 035009 [[1310.7945](#)].
- [104] G. Belanger, A. Mjallal and A. Pukhov, *WIMP and FIMP dark matter in the inert doublet plus singlet model*, *Phys. Rev. D* **106** (2022) 095019 [[2205.04101](#)].
- [105] A. Fradette and M. Pospelov, *BBN for the LHC: constraints on lifetimes of the Higgs portal scalars*, *Phys. Rev. D* **96** (2017) 075033 [[1706.01920](#)].
- [106] M. Pospelov and J. Pradler, *Big Bang Nucleosynthesis as a Probe of New Physics*, *Ann. Rev. Nucl. Part. Sci.* **60** (2010) 539 [[1011.1054](#)].
- [107] M. Duch, B. Grzadkowski and D. Huang, *Strongly self-interacting vector dark matter via freeze-in*, *JHEP* **01** (2018) 020 [[1710.00320](#)].
- [108] J.D. Clarke, R. Foot and R.R. Volkas, *Phenomenology of a very light scalar ($100 \text{ MeV} < m_h < 10 \text{ GeV}$) mixing with the SM Higgs*, *JHEP* **02** (2014) 123 [[1310.8042](#)].
- [109] K. Schmidt-Hoberg, F. Staub and M.W. Winkler, *Constraints on light mediators: confronting dark matter searches with B physics*, *Phys. Lett. B* **727** (2013) 506 [[1310.6752](#)].
- [110] MAGIC, FERMI-LAT collaboration, *Limits to Dark Matter Annihilation Cross-Section from a Combined Analysis of MAGIC and Fermi-LAT Observations of Dwarf Satellite Galaxies*, *JCAP* **02** (2016) 039 [[1601.06590](#)].
- [111] G. Alguero, G. Belanger, F. Boudjema, S. Chakraborti, A. Goudelis, S. Kraml et al., *micrOMEGAs 6.0: N-component dark matter*, *Comput. Phys. Commun.* **299** (2024) 109133 [[2312.14894](#)].
- [112] LZ collaboration, *First Dark Matter Search Results from the LUX-ZEPLIN (LZ) Experiment*, *Phys. Rev. Lett.* **131** (2023) 041002 [[2207.03764](#)].
- [113] XENON collaboration, *First Search for Light Dark Matter in the Neutrino Fog with XENONnT*, [2409.17868](#).

- [114] PANDAX collaboration, *PandaX-xT: a Multi-ten-tonne Liquid Xenon Observatory at the China Jinping Underground Laboratory*, [2402.03596](#).
- [115] L. Baudis, *Dual-phase xenon time projection chambers for rare-event searches*, *Phil. Trans. Roy. Soc. Lond. A* **382** (2023) 20230083 [[2311.05320](#)].
- [116] L. Baudis, *DARWIN/XLZD: A future xenon observatory for dark matter and other rare interactions*, *Nucl. Phys. B* **1003** (2024) 116473 [[2404.19524](#)].
- [117] FERMI-LAT collaboration, *Updated search for spectral lines from Galactic dark matter interactions with pass 8 data from the Fermi Large Area Telescope*, *Phys. Rev. D* **91** (2015) 122002 [[1506.00013](#)].
- [118] COSINE-100 collaboration, *Lowering threshold of NaI(Tl) scintillator to 0.7 keV in the COSINE-100 experiment*, *JINST* **19** (2024) P12013 [[2408.14688](#)].
- [119] PICO collaboration, *Dark Matter Search Results from the Complete Exposure of the PICO-60 C₃F₈ Bubble Chamber*, *Phys. Rev. D* **100** (2019) 022001 [[1902.04031](#)].
- [120] J.D. Lewin and P.F. Smith, *Review of mathematics, numerical factors, and corrections for dark matter experiments based on elastic nuclear recoil*, *Astropart. Phys.* **6** (1996) 87.
- [121] R.H. Helm, *Inelastic and Elastic Scattering of 187-Mev Electrons from Selected Even-Even Nuclei*, *Phys. Rev.* **104** (1956) 1466.
- [122] B.J. Kavanagh, T. Emken and R. Catena, *Measuring the local dark matter density in the laboratory*, *Phys. Rev. D* **104** (2021) 083023 [[2004.01621](#)].
- [123] P.F. de Salas and A. Widmark, *Dark matter local density determination: recent observations and future prospects*, *Rept. Prog. Phys.* **84** (2021) 104901 [[2012.11477](#)].
- [124] Y. Sofue, *Rotation Curve of the Milky Way and the Dark Matter Density*, *Galaxies* **8** (2020) 37 [[2004.11688](#)].
- [125] M.C. Smith et al., *The RAVE Survey: Constraining the Local Galactic Escape Speed*, *Mon. Not. Roy. Astron. Soc.* **379** (2007) 755 [[astro-ph/0611671](#)].
- [126] P.R. Kafle, S. Sharma, G.F. Lewis and J. Bland-Hawthorn, *On the Shoulders of Giants: Properties of the Stellar Halo and the Milky Way Mass Distribution*, *Astrophys. J.* **794** (2014) 59 [[1408.1787](#)].
- [127] R. Foot, *Hidden sector dark matter explains the DAMA, CoGeNT, CRESST-II and CDMS/Si experiments*, *Phys. Rev. D* **88** (2013) 025032 [[1209.5602](#)].
- [128] P.G. Staudt, J.S. Bullock, M. Boylan-Kolchin, D. Kirkby, A. Wetzel and X. Ou, *Sliding into DM: determining the local dark matter density and speed distribution using only the local circular speed of the galaxy*, *JCAP* **08** (2024) 022 [[2403.04122](#)].